

## Matrix product states algorithms and continuous systems

S. Iblisdir,<sup>1</sup> R. Orús,<sup>2</sup> and J. I. Latorre<sup>1</sup><sup>1</sup>*Department d'Estructura i Constituents de la Matèria, Universitat de Barcelona, 647 Diagonal, 08028 Barcelona, Spain*<sup>2</sup>*School of Physical Sciences, University of Queensland, QLD 4072, Australia*

(Received 27 October 2006; revised manuscript received 23 January 2007; published 23 March 2007)

A generic method to investigate many-body continuous-variable systems is pedagogically presented. It is based on the notion of matrix product states (so-called MPS's) and the algorithms thereof. The method is quite versatile and can be applied to a wide variety of situations. As a first test, we show how it provides reliable results in the computation of fundamental properties of a chain of quantum harmonic oscillators achieving off-critical and critical relative errors of the order of  $10^{-8}$  and  $10^{-4}$ , respectively. Next, we use it to study the ground-state properties of the quantum rotor model in one spatial dimension, a model that can be mapped to the Mott insulator limit of the one-dimensional Bose-Hubbard model. At the quantum critical point, the central charge associated with the underlying conformal field theory can be computed with good accuracy by measuring the finite-size corrections of the ground-state energy. Examples of MPS computations both in the finite-size regime and in the thermodynamic limit are given. The precision of our results is found to be comparable to that previously encountered in the MPS studies of, for instance, quantum spin chains. Finally, we present a spin-off application: an iterative technique to efficiently get numerical solutions of partial differential equations of many variables. We illustrate this technique by solving Poisson-like equations with precisions of the order of  $10^{-7}$ .

DOI: [10.1103/PhysRevB.75.104305](https://doi.org/10.1103/PhysRevB.75.104305)

PACS number(s): 71.10.Fd

### I. INTRODUCTION AND MAIN RESULTS

Generally, the behavior of quantum many-body systems cannot be grasped with a purely analytical approach—i.e., merely from the properties of its constituents. As a result, studying them often calls for approximation schemes that exhibit two features: (i) to provide an effective description of the system based on the identification of relevant degrees of freedom and (ii) to prescribe a (numerical) method to predict mean values of observables from this description. One such scheme is that based on the density matrix renormalization group (DMRG),<sup>1,2</sup> whose applications are countless (see, for example, Ref. 3 and references therein for a review).

Recently, a lot of attention has been devoted to regarding the DMRG from a quantum information perspective. The aim of this effort is twofold: first, to understand when and why the DMRG succeeds in describing a many-body system and, second, to improve and generalize the method. This program has met some success. We now understand better the relation between the difficulty to describe the state of a many-body system and the entanglement content of this state.<sup>4–6</sup> It is also clearer why the DMRG performs poorly in certain circumstances. The cases of spin chains with periodic boundary conditions<sup>7</sup> or two-dimensional spin lattices<sup>8</sup> are quite explicit in this respect. Many other interesting proposals have been made along those lines such as methods to simulate the evolution (in real or imaginary time) of a many-body system, both in the finite-size regime and in the thermodynamic limit,<sup>9–15</sup> or methods to efficiently compute a partition function.<sup>16</sup> The common notion underlying all this progress is that of matrix product states (MPS's) (Refs. 17–21)—that is, an ansatz that allows one to efficiently describe the state of the system when it is finitely correlated.

The present work is devoted to the study of many-body system with continuous degrees of freedom (or continuous-variable quantum many-body systems), using the MPS description and related algorithms. The main motivation of our work is to provide a tool that will eventually allow to study (1+1)-dimensional quantum field theories (similar work in this direction has been already considered in Refs. 22–24. The structure of this paper is as follows.

In Sec. II, we describe the procedure of local truncation of the Hilbert spaces of each subsystem for a generic model that allows to use the MPS machinery.

In Sec. III, we review several numerical techniques based on MPS's in a detailed and pedagogical way, both in the finite regime and in the thermodynamic limit.

In Sec. IV, we apply our methods to study a chain of coupled harmonic oscillators. This model is a lattice version of a (1+1)-dimensional Klein-Gordon field. We compute the energy, the von Neumann entropies of blocks, and correlators of the ground state. These computations allow us to proof our method.

Next, in Sec. V, we perform a detailed study of the one-dimensional quantum rotor model. This model is known to be interesting in studying the superfluid–Mott-insulator phase transitions or arrays of Josephson junctions.

In Sec. VI, we point out that the MPS algorithms may have applications well beyond the problems for which they have been initially designed. Namely, we show how they could be used to efficiently compute numerical solutions for a wide variety of partial differential equations.

Finally, in Sec. VII we summarize the conclusions of this work.

We wish to note that our proposal for treating continuous-variable systems with MPS's is qualitatively different from the Gaussian MPS's presented in Ref. 25.

## II. TRUNCATION OF LOCAL HILBERT SPACES IN A GENERIC MODEL

Let us consider an isolated system of  $N$  identical particles residing on some domain  $\mathcal{D}$  and are characterized, each, by a continuous degree of freedom  $x \in \mathcal{D}$ .

We suppose that the behavior of this system is exactly described by the Schrödinger equation, with a time-independent Hamiltonian  $H_{\text{exact}}$ . The ground state of this Hamiltonian reads

$$|\Psi_{0,\text{exact}}\rangle = \int dx_1 \dots dx_N \Psi_{0,\text{exact}}(x_1, \dots, x_N) |x_1, \dots, x_N\rangle. \quad (1)$$

The problem that we want to analyze is to find an approximation  $|\Psi_0\rangle$  of  $|\Psi_{0,\text{exact}}\rangle$  in the sense that  $E_0 = \langle \Psi_0 | H_{\text{exact}} | \Psi_0 \rangle$  is close to  $E_{0,\text{exact}} = \langle \Psi_{0,\text{exact}} | H_{\text{exact}} | \Psi_{0,\text{exact}} \rangle$ . For this, we will make two approximations. First, let us expand  $\Psi_0(x_1, \dots, x_N)$  in orthogonal sets of functions associated with each variable:

$$\Psi_{0,\text{exact}}(x_1, \dots, x_N) = \sum_{s_1 \dots s_N=1}^{\infty} c(s_1, \dots, s_N) \phi_{s_1}^{(1)}(x_1) \dots \phi_{s_N}^{(N)}(x_N). \quad (2)$$

We wish to consider two approximations of Eq. (2). The first one consists in an appropriate truncation on the dimension of the local Hilbert spaces. To be precise, for each particle  $k$ , we truncate the associated basis to a finite set of  $d$  orthonormal functions:

$$\Psi_{0,\text{exact}}(x_1, \dots, x_N) = \Psi_{0,d}(x_1, \dots, x_N) + \text{rest}_d. \quad (3)$$

In this paper we shall always consider this local dimension  $d$  to be the same for all particles. Notice that it is possible to make a clever choice of the local  $d$ -dimensional subspaces according to the particularities of the specific situation. In fact, once the relevant truncated subspaces are chosen, it is possible to make them depend on variational parameters which can be optimally tuned in order to minimize the error of the approximations. Furthermore, as long as we restrict our computations to the truncated basis,  $H_{\text{exact}}$  can be replaced by the truncated Hamiltonian

$$H = \sum_{i_1, \dots, i_N=1}^d \sum_{j_1, \dots, j_N=1}^d \langle \phi_{i_1}^{(1)} \otimes \dots \otimes \phi_{i_N}^{(N)} | H_{\text{exact}} | \phi_{j_1}^{(1)} \otimes \dots \otimes \phi_{j_N}^{(N)} \rangle | \phi_{i_1}^{(1)} \otimes \dots \otimes \phi_{i_N}^{(N)} \rangle \langle \phi_{j_1}^{(1)} \otimes \dots \otimes \phi_{j_N}^{(N)} |. \quad (4)$$

Considering Hamiltonians of the form

$$H_{\text{exact}} = \frac{1}{2} \sum_{i=1}^N T_i + \sum_{i,j=1}^N V(x_i, x_j), \quad (5)$$

we observe that  $H$  can always be given the standard form

$$H = \sum_{\gamma} \sum_{i=1}^N \otimes h_i^{\gamma}, \quad (6)$$

where  $h_i^{\gamma}$  is a Hermitian  $d \times d$  matrix acting on the local Hilbert space at site  $i$ . This fact might not be obvious for some interactions (think of the Coulomb interaction, for instance). We prove it as follows: suppose we have a potential term between two particles  $(i, j)$  whose matrix elements read

$$V_{(i_1 i_2), (j_1 j_2)} = \int dx_1 dx_2 \phi_{i_1}^*(x_1) \phi_{j_1}^*(x_2) V(x_1, x_2) \phi_{i_2}(x_1) \phi_{j_2}(x_2).$$

Performing the appropriate singular value decomposition, one gets

$$V_{(i_1 i_2), (j_1 j_2)} = \sum_{l=1}^{d^2} U_{(i_1 i_2), l} \Sigma_l W_{l, (j_1 j_2)}^*,$$

which is of the desired form.

The second approximation is to assume that the coefficients  $c(s_1, \dots, s_N)$  are given by a product of finite-size matrices. At this point, it is possible to choose among several prescriptions which indeed involve different numerical optimization algorithms. We will review three of them.

## III. MATRIX PRODUCT STATES AND OPTIMIZATION TECHNIQUES

Let us review briefly in this section some of the main numerical optimization techniques based on MPS's. Here we shall make a distinction among three different cases: namely, those of periodic boundary conditions, open boundary conditions, and the thermodynamic limit.

### A. Periodic boundary conditions

Let us associate  $d$  square matrices  $A(k, s_k)$  for each particle  $k=1, \dots, N$ . These matrices are assumed to have dimensions  $\chi \times \chi$ . The periodic boundary condition ansatz consists in assuming that the coefficient  $c(s_1, \dots, s_N)$  can be written, in terms of them, as

$$c(s_1, \dots, s_N) = \text{tr}(A(1, s_1) \dots A(N, s_N)). \quad (7)$$

It is sometimes convenient to use diagrammatic notations for tensors, where open indices are represented by open legs and contraction of indices is represented by gluing legs. The matrix elements  $A(k, s_k)_{\alpha_{k-1}, \alpha_k}$  at site  $k$  and the coefficient  $c(s_1, \dots, s_N)$  can then be represented as indicated in Fig. 1.

The representation given in Eq. (7) is efficient in the sense that it involves a relatively small number of independent parameters.<sup>7</sup> Indeed,  $O(d^N)$  independent parameters are necessary in order to describe such a general state as Eq. (3). In contrast, the MPS description requires only  $O(Nd\chi^2)$  parameters, which for fixed  $\chi$  is *linear* in  $N$ . The approximation (7) can be made arbitrarily precise upon taking  $\chi$  sufficiently large. Actually taking  $\chi = d^{\lfloor N/4 \rfloor}$  allows one to describe any state of  $N$  particles with local Hilbert spaces of dimension  $d^7$  within this prescription. But remarkably, for many Hamiltonians of physical interest,  $|\Psi_{0,\text{exact}}\rangle$  can be approximated ac-

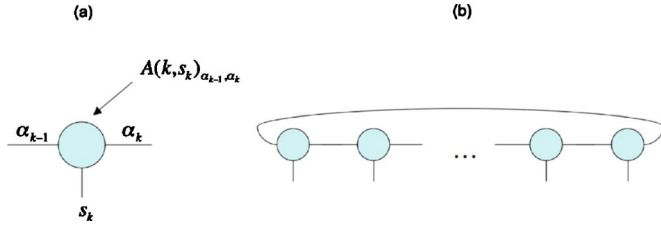


FIG. 1. (Color online) (a) Diagrammatic representation of the matrix element  $A(k, s_k)_{\alpha_{k-1}, \alpha_k}$  at site  $k$ . (b) Diagrammatic representation of the MPS structure of the coefficient  $c(s_1, \dots, s_N)$  (periodic boundary conditions).

curately with quite a modest value of  $\chi$ .<sup>6</sup> To be precise,  $\chi$  can be related to the entanglement entropy  $S$  of a subsystem in such a way that, for the case considered here,  $\chi \geq d^{S/2}$ . Hence, MPS's provide a faithful representation of the ground state of slightly correlated quantum mechanical systems, as is the case of noncritical one-dimensional quantum spin chains.<sup>5</sup>

In addition to providing an economical description of quantum states, MPS's also allow for an efficient computation of expectation values of observables. Indeed suppose that we want to compute the mean value of a tensor product of local observables  $\langle O_1 \otimes \dots \otimes O_N \rangle$ . One directly checks that the following identity holds:

$$\langle O_1 \otimes \dots \otimes O_N \rangle = \text{tr}(\hat{O}_1 \dots \hat{O}_N), \quad (8)$$

where  $\hat{O}_k = \sum_{s'_k, s_k=1}^d \langle s'_k | O_k | s_k \rangle \bar{A}(k, s'_k) \otimes A(k, s_k)$  is a transfer matrix for the local operator  $O_k$  at site  $k$  ( $\bar{A}$  denotes the conjugate matrix of  $A$ ). These quantities are diagrammatically represented in Fig. 2, and it is easy to see that in this case the computation of the mean value of a tensor product of local operators requires of a computational time which grows as  $O(Nd\chi^5)$ .

In order to compute an approximation to the ground state of the desired Hamiltonian operator  $H$ , the variational improvement now proceeds as follows. First, one sets all matrices  $A$  to some initial values. Then, one successively improves the matrices  $A$  related to particle 1, then those of particle 2, ..., then those of particle  $N$ , and then again. Sweeping sufficiently many times through the set  $\{1, \dots, N\}$ , one converges to a stationary value of the approximated ground-state energy  $E_0$ . The improvement of the matrices

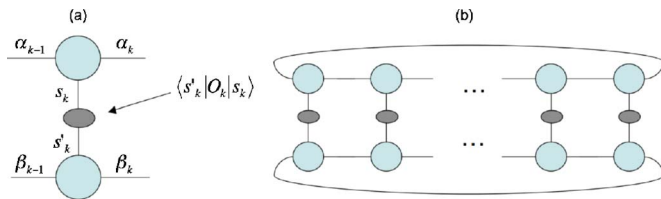


FIG. 2. (Color online) (a) The diagrammatic representation of the transfer matrix  $\hat{O}_k$  at site  $k$ . (b) The diagrammatic representation of the mean value  $\langle O_1 \otimes \dots \otimes O_N \rangle = \text{tr}(\hat{O}_1 \dots \hat{O}_N)$ , where the names of the indices are not explicitly indicated for simplicity.

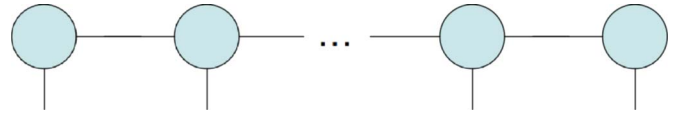


FIG. 3. (Color online) Diagrammatic representation of the MPS structure of the coefficient  $c(s_1, \dots, s_N)$  in terms of open boundary conditions.

related to particle  $k$  proceeds as follows. One computes the matrices  $\mathcal{H}^{(k)}$  (the effective Hamiltonian matrix) and  $\mathcal{N}^{(k)}$  (the normalization matrix) such that

$$\langle H \rangle = \sum_{s'_k, s_k=1}^d \sum_{\beta_{k-1}, \beta_k=1}^{\chi} \sum_{\alpha_{k-1}, \alpha_k=1}^{\chi} \bar{A}(k, s'_k)_{\beta_{k-1}, \beta_k} \times \mathcal{H}^{(k)}_{(s'_k \beta_{k-1} \beta_k), (s_k \alpha_{k-1} \alpha_k)} A(k, s_k)_{\alpha_{k-1}, \alpha_k}, \quad (9)$$

$$\langle \Psi_0 | \Psi_0 \rangle = \sum_{s'_k, s_k=1}^d \sum_{\beta_{k-1}, \beta_k=1}^{\chi} \sum_{\alpha_{k-1}, \alpha_k=1}^{\chi} \bar{A}(k, s'_k)_{\beta_{k-1}, \beta_k} \times \mathcal{N}^{(k)}_{(s'_k \beta_{k-1} \beta_k), (s_k \alpha_{k-1} \alpha_k)} A(k, s_k)_{\alpha_{k-1}, \alpha_k}. \quad (10)$$

The computation of both  $\mathcal{H}^{(k)}$  and  $\mathcal{N}^{(k)}$  follows the same rules as the computation of expected values in terms of transfer matrices and is straightforward by using the tensor network diagrammatic representation from Fig. 2 removing from the diagram the appropriate matrices at site  $k$ , given that  $H$  has been brought to a normal form (6). Extremizing  $\langle H \rangle$  with the constraint  $\langle \Psi_0 | \Psi_0 \rangle = 1$  with respect to the coefficients  $\bar{A}(k, s_k)_{\alpha_{k-1}, \alpha_k}$  leads to having to solve the (generalized) eigenvalue problem

$$\sum_{s'_k=1}^d \sum_{\alpha_{k-1}, \alpha_k=1}^{\chi} [\mathcal{H}^{(k)}_{(s'_k \beta_{k-1} \beta_k), (s_k \alpha_{k-1} \alpha_k)} - \lambda \mathcal{N}^{(k)}_{(s'_k \beta_{k-1} \beta_k), (s_k \alpha_{k-1} \alpha_k)}] \times A(k, s_k)_{\alpha_{k-1}, \alpha_k} = 0, \quad \forall s'_k, \beta_{k-1}, \beta_k, \quad (11)$$

where a Lagrange multiplier  $\lambda$  has been introduced. The value of this Lagrange multiplier is actually the value of the ground-state energy, as computed at the considered step of the algorithm.

## B. Open boundary conditions

We assume again an ansatz of the form (7) but where the matrices now have different sizes, depending on the site to which they are related. The matrices  $A(1, s)$  have size  $1 \times \chi$ , the matrices  $A(k, s)$ ,  $k=2, \dots, N-1$ , have size  $\chi \times \chi$ , and the matrices  $A(N, s)$  have size  $\chi \times 1$ . This matrix product structure can again be represented in terms of a diagrammatic tensor network, as shown in Fig. 3.

As in the case of periodic boundary conditions, this MPS description is efficient as compared to the exact description of the  $d^N$  coefficients  $c(s_1, \dots, s_N)$ . Again, we need  $O(Nd\chi^2)$  parameters to describe the appropriate product of matrices, which can be made as precise as desired by increasing the parameter  $\chi$ . In this case, it is easy to see by considering the

consecutive Schmidt decompositions of the system that if  $\chi = d^{\lfloor N/2 \rfloor}$ , then any state of  $N$  particles of local dimensionality  $d$  can be represented.

Working with open boundary conditions is a stronger assumption than working with periodic ones. It is also a less physical approximation when studying systems described by a translationally invariant Hamiltonian. However, they allow one to reparametrize the MPS's in a manner that considerably lowers the computational cost of each step of the optimization procedure. This can be achieved thanks to the local gauge freedom existing in the definition (7). Let  $T_k$  denote a  $\chi \times \chi$  invertible matrix. The transformation  $A(k, s) \rightarrow A(k, s)T_k$ ,  $A(k+1, s) \rightarrow T_k^{-1}A(k+1, s)$  ( $k < N$ ) leaves invariant the state described by the MPS's.

We start with site 1 and perform the singular value decomposition

$$A(1, s_1)_{1, \alpha_1} = \sum_{\lambda, \mu=1}^{\min(d, \chi)} U_{s_1, \lambda}^{(1)} \Sigma_{\lambda, \mu}^{(1)} V_{\mu, \alpha_1}^{(1)}, \quad (12)$$

where by definition of the singular value decomposition  $\Sigma^{(1)}$  is a diagonal  $\min(d, \chi) \times \min(d, \chi)$  matrix, and  $U^{(1)}$  and  $V^{(1)}$  satisfy  $U^{(1)\dagger}U^{(1)} = I_{\min(d, \chi)}$  and  $V^{(1)}V^{(1)\dagger} = I_{\min(d, \chi)}$ . We then perform a gauge transformation

$$A(1, s_1)_{1, \alpha_1} \rightarrow U(1, s_1)_{1, \lambda} \equiv U_{s_1, \lambda}^{(1)},$$

$$A(2, s_2)_{\alpha_1, \alpha_2} \rightarrow B(2, s_2)_{\lambda, \alpha_2} = \sum_{\mu=1}^{\min(d, \chi)} \sum_{\nu=1}^{\chi} \Sigma_{\lambda, \mu}^{(1)} V_{\mu, \nu}^{(1)} A(2, s_2)_{\nu, \alpha_2}.$$

Observe that the dimensions of the matrices related to sites 1 and 2 may change along this transformation. Then we perform the further singular value decomposition for  $B(2, s_2)$ ,

$$B(2, s_2)_{\lambda, \alpha_2} = \sum_{\mu, \nu=1}^{\min(d^2, \chi)} U_{(s_2 \lambda), \mu}^{(2)} \Sigma_{\mu, \nu}^{(2)} V_{\nu, \alpha_2}^{(2)},$$

and make the gauge transformation

$$B(2, s_2)_{\lambda, \alpha_2} \rightarrow U(2, s_2)_{\lambda, \mu} \equiv U_{(s_2 \lambda), \mu}^{(2)},$$

$$\begin{aligned} A(3, s_3)_{\alpha_2, \alpha_3} &\rightarrow B(3, s_3)_{\mu, \alpha_3} \\ &= \sum_{\nu=1}^{\min(d^2, \chi)} \sum_{\alpha_2=1}^{\chi} \Sigma_{\mu, \nu}^{(2)} V_{\nu, \alpha_2}^{(2)} A(3, s_3)_{\alpha_2, \alpha_3}. \end{aligned}$$

Iterating this procedure up to site  $k-1$ , the state is represented through the product of matrices

$$U(1, s_1) \cdots U(k-1, s_{k-1}) B(k, s_k) A(k+1, s_{k+1}) \cdots A(N, s_N). \quad (13)$$

Then, one applies the same procedure, starting from site  $N$ , up to site  $k+1$  this time, keeping at each step the matrix at the right of the singular decomposition. Eventually, our state is described by a product of matrices of the form

$$U(1, s_1) \cdots U(k-1, s_{k-1}) A(k, s_k) V(k+1, s_{k+1}) \cdots V(N, s_N). \quad (14)$$

The principal virtue of this gauge is that  $\langle \Psi_0 | \Psi_0 \rangle$  now assumes a simple form, namely,

$$\langle \Psi_0 | \Psi_0 \rangle = \sum_{s_k=1}^d \text{tr}(A^*(k, s_k) A(k, s_k)), \quad (15)$$

so that the corresponding normalization matrix  $\mathcal{N}^{(k)}$  is now equal to the identity. This specific property of the chosen MPS representation for open boundary conditions allows a more straightforward numerical analysis of the corresponding variational optimization algorithm to compute good approximations of the ground state of Hamiltonians. The variational improvement proceeds now by sweeping back and forth over the  $N$  sets of matrices of the MPS's optimizing over a particular site at each step. However, when optimizing over the set of matrices at site  $k$ , we shall consider now the MPS representation for open boundary conditions in terms of matrices  $U(l, s_l)$  for sites  $l=1, 2, \dots, k-1$ ,  $V(l, s_l)$  for sites  $l=k+1, k+2, \dots, N$ , and  $A(k, s_k)$ . The corresponding generalized eigenvalue problem is then transformed into a simple eigenvalue problem. Therefore, computing the ground state of the corresponding effective Hamiltonian  $\mathcal{H}^{(k)}$  directly gives the variational ground-state energy when optimizing over the site  $k$ , together with the corresponding well-normalized optimal matrix for that site. This can be very efficiently computed by means of large sparse-matrix techniques. Moving from site  $k$  to site  $k+1$  then proceeds by means of evaluating the new representation of the MPS's in terms of  $U(l, s_l)$  for sites  $l=1, 2, \dots, k$ ,  $V(l, s_l)$  for sites  $l=k+2, k+3, \dots, N$ , and  $A(k+1, s_{k+1})$ , which only involves performing the appropriate singular value decomposition over the just-obtained optimal matrix at site  $k$ . As a matter of fact, the computation of  $\mathcal{H}^{(k)}$  at each step (as well as the computation of expected values of local observables) is also very much simplified thanks to the considered structure of the open boundary MPS's, taking into account the normalization conditions from the left and from the right of the matrices forming the MPS's.

Finally, it is easy to see that considering the above procedures, together with efficient clever contractions of the different tensor networks that appear in the calculations, the computational running time of the variational optimization algorithm over MPS's with open boundary conditions grows like  $O(N^2 d \chi^3)$ .

Let us now present an alternative derivation of the MPS structure for open boundary conditions.<sup>4</sup> If we perform the Schmidt decomposition between the local system 1 and the remaining  $N-1$ , we can write the state as

$$|\Psi_0\rangle = \sum_{\alpha_1=1}^{\min(d, \chi)} \lambda(1)_{\alpha_1} |\tau_{\alpha_1}^{(1)}\rangle |\tau_{\alpha_1}^{(2 \cdots n)}\rangle, \quad (16)$$

where  $\lambda(1)_{\alpha_1}$  are the Schmidt coefficients and  $|\tau_{\alpha_1}^{(1)}\rangle$  and  $|\tau_{\alpha_1}^{(2 \cdots n)}\rangle$  are the corresponding left and right Schmidt vectors. Expressing the left Schmidt vector in terms of the original



local basis for system 1,  $|\Psi_0\rangle$  can then be written as

$$|\Psi_0\rangle = \sum_{s_1=1}^d \sum_{\alpha_1=1}^{\min(d,\chi)} \Gamma(1,s_1)_{1\alpha_1} \lambda(1)_{\alpha_1} |\phi_{s_1}^{(1)}\rangle |\tau_{\alpha_1}^{(2\cdots n)}\rangle, \quad (17)$$

where  $\Gamma(1,s_1)_{1\alpha_1}$  is the appropriate coefficients of the change of basis. That is,  $|\tau_{\alpha_1}^{(1)}\rangle = \sum_{s_1} \Gamma(1,s_1)_{1\alpha_1} |\phi_{s_1}^{(1)}\rangle$ . At this point, we expand each Schmidt vector  $|\tau_{\alpha_1}^{(2\cdots n)}\rangle$  in the original local basis for system 2—that is

$$|\tau_{\alpha_1}^{(2\cdots n)}\rangle = \sum_{s_2=1}^d |\phi_{s_2}^{(2)}\rangle |\omega_{\alpha_1 s_2}^{(3\cdots n)}\rangle. \quad (18)$$

We now write the unnormalized quantum state  $|\omega_{\alpha_1 s_2}^{(3\cdots n)}\rangle$  in terms of the at most  $d^2$  eigenvectors of the joint reduced density matrix for systems  $(3, \dots, n)$ —that is, in terms of the right Schmidt vectors  $|\tau_{\alpha_2}^{(3\cdots n)}\rangle$  of the particular bipartition between the first two local systems and the rest, together with the corresponding Schmidt coefficients  $\lambda(2)_{\alpha_2}$ :

$$|\omega_{\alpha_1 s_2}^{(3\cdots n)}\rangle = \sum_{\alpha_2=1}^{\min(d^2,\chi)} \Gamma(2,s_2)_{\alpha_1 \alpha_2} \lambda(2)_{\alpha_2} |\tau_{\alpha_2}^{(3\cdots n)}\rangle. \quad (19)$$

Placing the last two expressions into Eq. (17) we get

$$|\Psi_0\rangle = \sum_{s_1, s_2=1}^d \sum_{\alpha_1=1}^{\min(d,\chi)} \sum_{\alpha_2=1}^{\min(d^2,\chi)} \Gamma(1,s_1)_{1\alpha_1} \lambda(1)_{\alpha_1} \times \Gamma(2,s_2)_{\alpha_1 \alpha_2} \lambda(2)_{\alpha_2} |\phi_{s_1}^{(1)}\rangle \otimes |\phi_{s_2}^{(2)}\rangle |\tau_{\alpha_2}^{(3\cdots n)}\rangle. \quad (20)$$

Iterating the above procedure, we finally get a representation of the quantum state in terms of some tensors  $\Gamma$  and some vectors  $\lambda$ :

$$|\Psi_{0,d}\rangle = \sum_{\{s\}} \sum_{\{\alpha\}} \Gamma(1,s_1)_{1\alpha_1} \lambda(1)_{\alpha_1} \Gamma(2,s_2)_{\alpha_1 \alpha_2} \times \lambda(2)_{\alpha_2} \dots \lambda(N-1)_{\alpha_{N-1}} \Gamma(N,s_N)_{\alpha_{N-1} 1} \times |\phi_{s_1}^{(1)}\rangle |\phi_{s_2}^{(2)}\rangle \dots |\phi_{s_N}^{(N)}\rangle, \quad (21)$$

where the whole set of indices  $\{s\}$  and  $\{\alpha\}$  are added up to their respective allowed values.

The above decomposition immediately provides the Schmidt vectors  $\lambda$  of all the possible contiguous bipartitions of the system. In fact, Eq. (21) is indeed a reparametrization of an open boundary condition MPS, in a gauge where

$$A(k,s_k)_{\alpha_{k-1}\alpha_k} \equiv \Gamma(k,s_k)_{\alpha_{k-1}\alpha_k} \lambda(k)_{\alpha_k}. \quad (22)$$

This reparametrization of the MPS is diagrammatically represented in Fig. 4. We also see that the maximum allowed rank of the different indices  $\alpha_k$ ,  $k=1, \dots, N-1$ , is site dependent, since the size of the Hilbert spaces considered when performing the consecutive Schmidt decompositions depends on the site. In particular, we have that, at most,  $\alpha_k = 1, 2, \dots, d^k$  for  $k=0, 1, \dots, \lfloor N/2 \rfloor$  and  $\alpha_k = 1, 2, \dots, d^{(N-k)}$  for  $k=N, N-1, \dots, \lfloor N/2 \rfloor + 1$ . The value of the true rank of the indices in the MPS comes dictated by the minimum between these quantities and the parameter  $\chi$ .

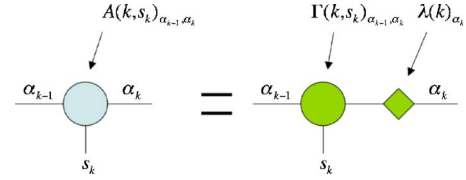


FIG. 4. (Color online) The diagrammatic representation of the decomposition of  $A(k,s_k)$  into a tensor  $\Gamma(k,s_k)$  and a Schmidt coefficient  $\lambda(k)$ .

In practice, when studying physically relevant states, many of the Schmidt coefficients for the different contiguous bipartitions of the system shall be (almost) equal to zero, depending on the particular state being considered. One is then interested in bounding the range of the indices by a number  $\chi$ , which now is clearly understood as a measure of the maximum contiguous bipartite entanglement in the system, since it is the maximum allowed Schmidt number for a contiguous bipartition in our MPS decomposition. Notice that this truncation in the Schmidt ranks imposes a strict restriction on the maximal amount of entanglement entropy that the ansatz can handle. To be precise, if  $S = -\text{tr}(\rho \log_2 \rho)$  is the von Neumann entropy corresponding to the reduced density matrix describing one of the subsystems of a bipartition of the quantum state into two contiguous pieces, then we see that  $S \leq \log_2 \chi$ . This property makes these states to be *finitely correlated*.

### C. Thermodynamic limit for translationally invariant systems

In the case of a translationally invariant system, the techniques described in the foregoing analysis can be extended so as to consider an infinite number of particles, which allows us to get rid of finite-size effects.<sup>13</sup> We now assume that all the properties of the state are defined in terms of a single set of matrices  $A(s) \equiv \Gamma(s)\lambda$  which now do not depend on the position.

It is indeed possible to perform the evolution of such an MPS in the thermodynamic limit both in real and Euclidean time as driven by a translationally invariant Hamiltonian, as originally explained in Ref. 13. To this end, let us assume now that our Hamiltonian is a translationally invariant infinite sum of interaction terms which only involve nearest-neighbor interactions,

$$H = \sum_k h^{(k,k+1)}. \quad (23)$$

The evolution operator  $e^{-iHt}$  is now decomposed by means of a Suzuki-Trotter decomposition<sup>26</sup> in terms of unitary gates acting only on two sites:

$$U^{(k,k+1)} = e^{-ih^{(k,k+1)}\delta t}, \quad (24)$$

where  $\delta t \ll 1$  and which have to be applied  $t/\delta t$  times. Arranging the above gates into two mutually noncommuting pieces

$$U(AB) \equiv \otimes_k U^{(2k,2k+1)}, \quad U(BA) \equiv \otimes_k U^{(2k-1,2k)}, \quad (25)$$

we can compute the evolution in the MPS by slightly breaking the translational invariance as follows: since the set of

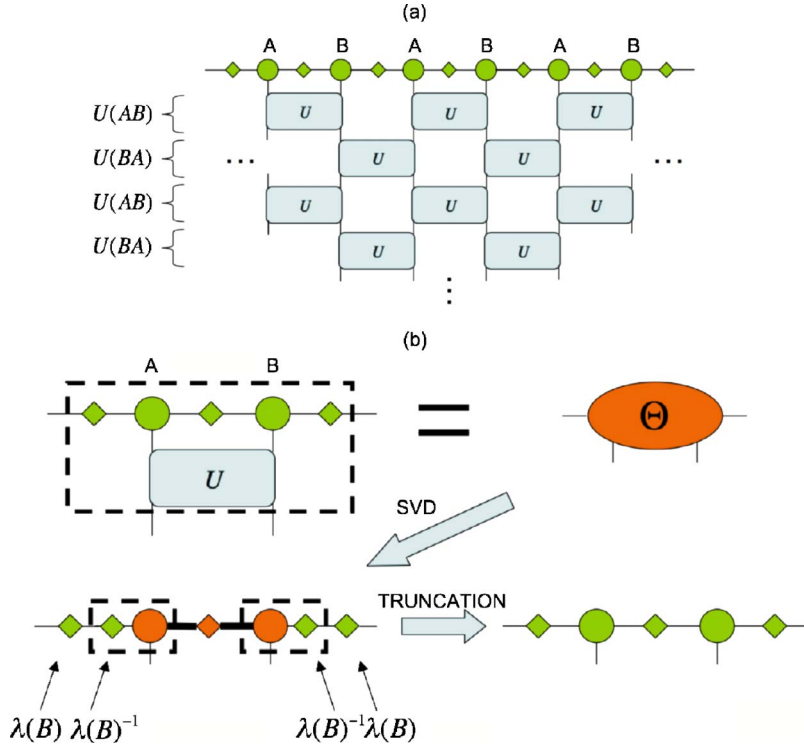


FIG. 5. (Color online) (a) The sequential application of two-particle unitary gates to the MPS structure. (b) The updating rule for the MPS in the thermodynamic limit under the action of a two-particle gate follows the singular value decomposition (SVD) of the composed tensor and a local truncation up to  $\chi$  of the common index between the two particles. After the singular value decomposition, the vectors  $\lambda$  are properly inserted by hand on the two sides in order to preserve the MPS structure, which also changes the values of the tensors at A and B by a factor of  $\lambda^{-1}$ .

gates in  $U(AB)$  can be applied at once [the same holds for those in  $U(BA)$ ], we consider an MPS invariant under shifts of two lattice sites, so that

$$\Gamma(2k, s_{2k}) = \Gamma(A, s_A), \quad \Gamma(2k+1, s_{2k+1}) = \Gamma(B, s_B) \quad (26)$$

and

$$\lambda(2k) = \lambda(A), \quad \lambda(2k+1) = \lambda(B), \quad (27)$$

for all the possible values of  $k$ . The updating of the MPS along the time evolution is then dictated by sequentially updating matrices for the A and B sites according to the application of the gates in Eq. (25). As explained in Ref. 13, the updating rule for the matrices of the MPS once a two-particle unitary gate is applied can be done by means of the appropriate singular value decomposition followed by a truncation up to  $\chi$  of the rank of the common index that joins the matrices at the two sites.

Let us be more precise with the above statement. In the situation in which a two-body gate  $U^{(A,B)}$  from Eq. (24) is applied over two consecutive sites A and B, the updating procedure starts with the following tensor contraction:

$$\Theta(s'_A, s'_B) \equiv \sum_{s_A=1}^d \sum_{s_B=1}^d U^{(A,B)}(s'_A, s'_B; s_A, s_B) \times \lambda(B) \Gamma(A, s_A) \lambda(A) \Gamma(B, s_B) \lambda(B). \quad (28)$$

By performing the singular value decomposition of the above tensor with respect to the left and right indices, we get

$$\Theta(s'_A, s'_B) = A(s'_A) \lambda'(A) B(s'_B) = \lambda(B) \Gamma'(A, s'_A) \lambda'(A) \Gamma'(B, s'_B) \lambda(B), \quad (29)$$

where  $\Gamma'(A, s'_A) \equiv \lambda^{-1}(B) A(s'_A)$  and  $\Gamma'(B, s'_B) \equiv B(s'_B) \lambda^{-1}(B)$ ,

respectively, correspond to the updated new matrices for sites A and B. The last step in the updating procedure comes dictated by a truncation in the eigenvalues  $\lambda'(A)$ , in such a way that the final size of the updated matrices is again  $\chi \times \chi$ . The sequential application of gates and the truncation scheme are diagrammatically represented in Fig. 5.

Following this updating rule, it is possible to compute the evolution in time of any MPS in the thermodynamic limit as driven by a Hamiltonian such as the one from Eq. (23) in  $O(d^3 \chi^3)$  time. Also, by performing evolution in Euclidean time and taking very good care of the normalization of the wave function at each computational step, it is possible to find MPS approximations to the ground state of a wide variety of interacting Hamiltonians such as the ones considered in this paper. Note the difference between this optimization procedure, based on Euclidean time evolution in the thermodynamic limit, and the ones described for finite systems in terms of local optimizations of the matrices by performing sweeps over the different particles, which involved the solution to (generalized) eigenvalue problems.

#### IV. BENCHMARK: THE HARMONIC CHAIN

As an illustration of the above methods, we consider an open chain of spin-0 particles interacting via the Hamiltonian

$$H_{\text{exact}} = \frac{1}{2} \sum_{i=1}^N p_i^2 + \mu \sum_{i=1}^N x_i^2 + \Lambda \sum_{i=1}^{N-1} (x_i - x_{i+1})^2, \quad (30)$$

corresponding to the well-known case of interacting harmonic systems<sup>22,23,27-30</sup> and which is critical in the thermodynamic limit for  $\mu=0$ . A remarkable feature of this Hamiltonian is obtained upon considering the continuous limit

$$\lim_{N \rightarrow \infty} \lim_{\Lambda \rightarrow \infty} H_{\text{exact}} \approx \int dq (\partial_\nu \partial^\nu + m^2) \varphi(q), \quad (31)$$

where we have made the identification  $i \rightarrow q$ ,  $x \rightarrow \varphi$ ,  $\mu \rightarrow m^2$ , and which corresponds to the usual Klein-Gordon Hamiltonian of a free spinless field  $\varphi$ .

The ground state of  $H_{\text{exact}}$  and its associated energy  $|\Psi_{0,\text{exact}}\rangle$  and  $E_{0,\text{exact}}$  can be analytically computed.<sup>31</sup> Rewriting  $H_{\text{exact}}$  as

$$H_{\text{exact}} = \frac{1}{2} \sum_{i=1}^N p_i^2 + \sum_{i,j=1}^N x_i K_{i,j} x_j, \quad (32)$$

we have  $\Psi_{0,\text{exact}}(x_1, \dots, x_N) = C \exp[-\sum_{i,j=1}^N x_i (\sqrt{K})_{ij} x_j]$ ,  $C$  being a normalization constant, and  $E_{0,\text{exact}} = \frac{1}{2} \text{tr}(\sqrt{K})$ . This result will allow us to estimate the accuracy of our calculations.

Let us now apply the methods discussed in the previous sections and search for an MPS approximation to the ground state. As basis functions, we have chosen to use, for all particles, the (truncated) spectrum of a single harmonic oscillator: that is,

$$\phi_j(x) = C_j e^{-a^2 x^2/2} \mathcal{H}_j(ax), \quad j = 0, \dots, d-1. \quad (33)$$

In this expression,  $C_j$  is a normalization constant,  $\mathcal{H}_j$  denotes the degree- $j$  Hermite polynomial, and  $a = (2\mu)^{1/4}$  (notice that we could also keep  $a$  as an external variational parameter). With this choice  $H_{\text{exact}}$  can be approximated by the truncated Hamiltonian

$$H = \frac{1}{2} \sum_{k=1}^N \tau^{(k)} + (\Lambda + \mu)(\zeta^{(1)} + \zeta^{(N)}) + (2\Lambda + \mu) \sum_{k=2}^{N-1} \zeta^{(k)} - 2\Lambda \sum_{k=1}^{N-1} \eta^{(k)} \eta^{(k+1)}, \quad (34)$$

where  $\tau$ ,  $\zeta$ , and  $\eta$  are Hermitian matrices defined as

$$\begin{aligned} \tau_{m,n} &= - \int dx \phi_m(x) \frac{d^2}{dx^2} \phi_n(x), \\ \zeta_{m,n} &= \int dx \phi_m(x) x^2 \phi_n(x), \\ \eta_{m,n} &= \int dx \phi_m^{(i)}(x) x \phi_n(x), \end{aligned} \quad (35)$$

where  $m, n = 0, \dots, d-1$ . Analytical expressions for the entries of the matrices  $\tau$ ,  $\zeta$ , and  $\eta$  are straightforwardly derived from the elementary properties of Hermite polynomials (see Ref. 32). The Hamiltonian (33) is now of the form (6), so that its properties can be investigated with the algorithms of the previous sections. To be precise, we show here the performance of the finite-size numerical optimization algorithms for a system of  $N=30$  sites and open boundary conditions, for several values of the external parameters. Notice that our simulations allow us to change both  $d$  and  $\chi$  independently.

TABLE I. Performances of the MPS algorithm for computing the ground-state energy of the harmonic chain, both in the off-critical regime ( $\mu=1$ ) and close to criticality ( $\mu=10^{-6}$ ).  $N$  denotes the number of variables,  $d$  denotes the number of local levels,  $\chi$  is the dimension of the matrices of the MPS ansatz, and  $\delta$  is the relative error.

$N$	$d$	$\chi$	$\delta(\mu=1)$	$\delta(\mu=10^{-6})$
30	4	5	$8.27 \times 10^{-3}$	$5.38 \times 10^{-3}$
30	4	10	$8.27 \times 10^{-3}$	$5.23 \times 10^{-3}$
30	4	15	$8.27 \times 10^{-3}$	$5.23 \times 10^{-3}$
30	4	20	$8.27 \times 10^{-3}$	$5.23 \times 10^{-3}$
30	4	25	$8.27 \times 10^{-3}$	$5.23 \times 10^{-3}$
30	6	5	$5.95 \times 10^{-4}$	$3.07 \times 10^{-3}$
30	6	10	$5.95 \times 10^{-4}$	$1.71 \times 10^{-3}$
30	6	15	$5.95 \times 10^{-4}$	$1.68 \times 10^{-3}$
30	6	20	$5.95 \times 10^{-4}$	$1.67 \times 10^{-3}$
30	6	25	$5.95 \times 10^{-4}$	$1.67 \times 10^{-3}$
30	8	5	$4.03 \times 10^{-5}$	$3.01 \times 10^{-3}$
30	8	10	$4.01 \times 10^{-5}$	$1.04 \times 10^{-3}$
30	8	15	$4.01 \times 10^{-5}$	$8.65 \times 10^{-4}$
30	8	20	$4.01 \times 10^{-5}$	$8.48 \times 10^{-4}$
30	8	25	$4.01 \times 10^{-5}$	$8.46 \times 10^{-4}$
30	10	5	$2.82 \times 10^{-6}$	$2.94 \times 10^{-3}$
30	10	10	$2.63 \times 10^{-6}$	$9.36 \times 10^{-4}$
30	10	15	$2.63 \times 10^{-6}$	$6.46 \times 10^{-4}$
30	10	20	$2.63 \times 10^{-6}$	$5.34 \times 10^{-4}$
30	10	25	$2.63 \times 10^{-6}$	$5.24 \times 10^{-4}$
30	12	5	$3.63 \times 10^{-7}$	$3.06 \times 10^{-3}$
30	12	10	$1.73 \times 10^{-7}$	$9.47 \times 10^{-4}$
30	12	15	$1.72 \times 10^{-7}$	$5.72 \times 10^{-4}$
30	12	20	$1.72 \times 10^{-7}$	$4.4 \times 10^{-4}$
30	12	25	$1.72 \times 10^{-7}$	$3.70 \times 10^{-4}$
30	14	5	$2.05 \times 10^{-7}$	$2.98 \times 10^{-3}$
30	14	10	$1.42 \times 10^{-8}$	$9.07 \times 10^{-4}$
30	14	15	$1.41 \times 10^{-8}$	$5.60 \times 10^{-4}$
30	14	20	$1.41 \times 10^{-8}$	$3.75 \times 10^{-4}$
30	14	25	$1.41 \times 10^{-8}$	$3.21 \times 10^{-4}$

### A. Relative error of the ground-state energy

We have performed computations of an approximated ground state of the system and compared the obtained results with the exact ones, for several values of  $d$  and  $\chi$ . Our comparison is made precise by means of calculating the relative error of the ground-state energy, as measured by the quantity

$$\delta \equiv \left| \frac{E_0 - E_{0,\text{exact}}}{E_{0,\text{exact}}} \right|. \quad (36)$$

In the off-critical regime ( $\mu \neq 0$ ), it is seen in Table I that the relative error of the ground-state energy decreases exponentially with  $d$  down to  $10^{-8}$ , while it remains very stable for the considered values of  $\chi$ . On the other hand, the exponential behavior of the relative error as a function of  $d$  becomes

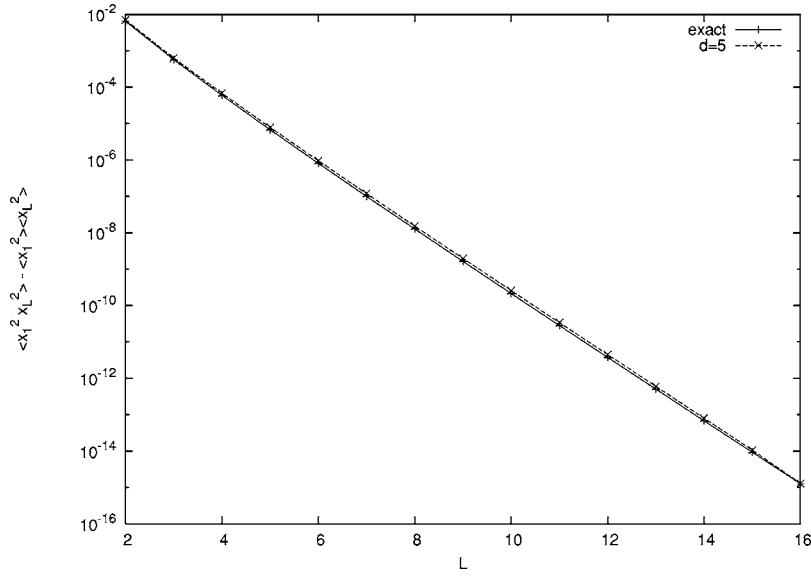


FIG. 6. Off-critical correlator  $C(L) = \langle x_1^2 x_L^2 \rangle - \langle x_1^2 \rangle \langle x_L^2 \rangle$  for  $N=30$  and  $\mu=1$ . The numerical computations have been done for  $N=30$ ,  $\chi=30$ , and  $d=5$ . Very good agreement with the exact value is observed to appear.

weaker when close to the criticality, as can be observed also in Table I, where it decreases up to  $10^{-4}$ . Let us remark that the precisions that we find in our calculations are in agreement and can compete with those found in previous numerical analyses of the harmonic chain.<sup>23,28–30</sup>

### B. Off-critical correlator

Our numerical calculations allow us to compare the performance of the simulation technique by means of considering the correlation functions of the system. To be precise, we have numerically computed the two-point correlation function

$$C(L) = \langle x_1^2 x_L^2 \rangle - \langle x_1^2 \rangle \langle x_L^2 \rangle, \quad (37)$$

for  $N=30$ ,  $\chi=30$ , and  $d=5$ , and compared it to its exact value. It is a fact that, when close to criticality, the correlators are not well reproduced by means of our MPS techniques (which inherently make use of a finite correlation

length). However, away from criticality ( $\mu=1$ ), our algorithms provide good approximations of the correlation functions, as can be seen in Fig. 6, where it is shown that the numerical results obtained for  $C(L)$  agree very well with the exact value.

### C. Absolute error of the entanglement entropy

Recently, a lot of attention has been devoted to computing the entanglement present in Gaussian systems (see, for instance Ref. 27, and references therein). This motivated us to look at the entanglement entropy  $S = -\text{tr}(\rho \log_2 \rho)$  of the ground-state reduced density matrix  $\rho$  of half the open chain as a further test of our method. We have computed  $S$  for  $\chi=10$ ,  $d=14$ , and  $\Lambda=0.5$ , as a function of the parameter  $\mu^2$  and compared it to the exact case. As can be seen in Fig. 7, the absolute error decreases superexponentially when departing from the critical region, easily achieving values of the order of  $10^{-9}$  when being sufficiently away from criticality

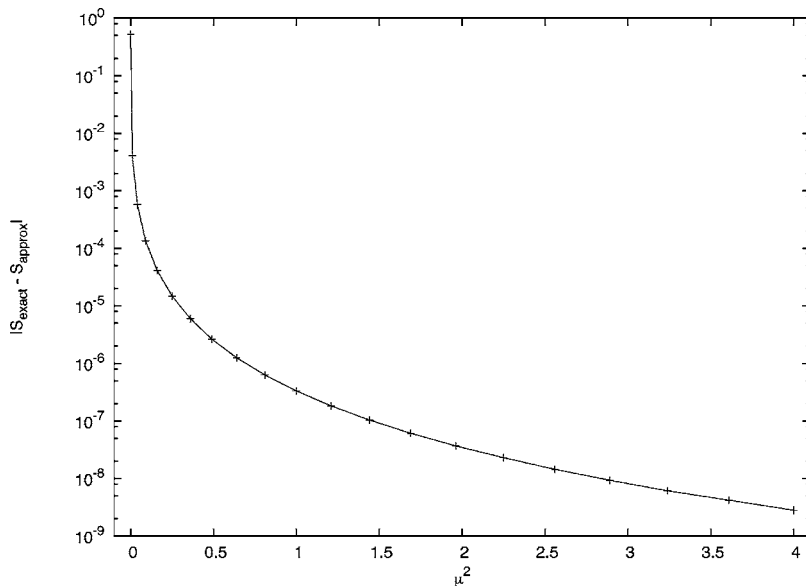


FIG. 7. Absolute error in the entanglement entropy for the harmonic chain for  $N=30$ ,  $d=14$ ,  $\chi=10$ , and  $\Lambda=0.5$ , as a function of  $\mu^2$ .



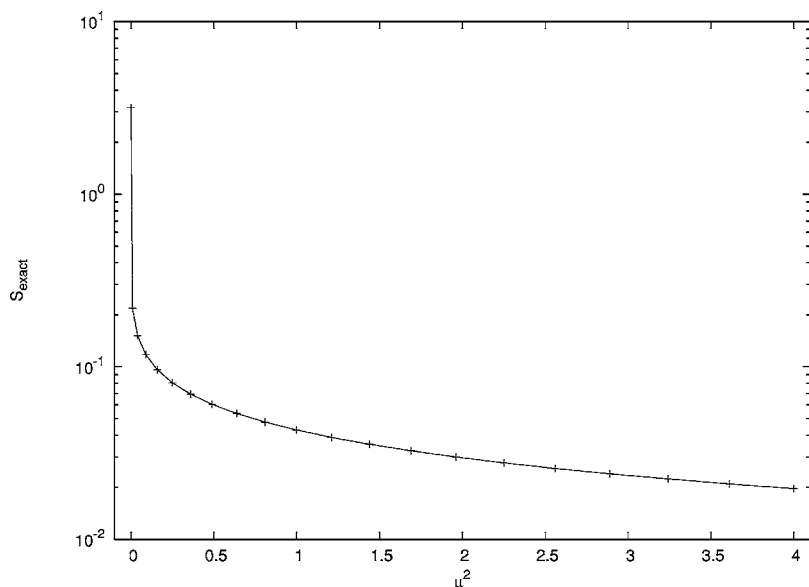


FIG. 8. Exact entanglement entropy for the harmonic chain for  $N=30$  and  $\Lambda=0.5$ , as a function of  $\mu^2$ .

and giving small relative deviations from the exact entropy in Fig. 8.

### V. ONE-DIMENSIONAL QUANTUM ROTOR

As a further example of the application of the techniques presented in the previous sections, we consider here the properties of the ground state of the so-called quantum rotor model in one spatial dimension. This continuous-variable model is defined by means of the Hamiltonian

$$H_{\text{exact}} = \sum_{k=1}^N \left( -2J \cos(\theta_k - \theta_{k+1}) - \frac{U}{2} \frac{\partial^2}{\partial \theta_k^2} \right), \quad (38)$$

where the angles  $\theta_k \in [0, 2\pi) \forall k$  and  $U, J$  are external parameters. The above Hamiltonian accurately describes the behavior within the Mott insulator regime of the one-dimensional Bose-Hubbard model, where small fluctuations

around the mean number of atoms per site can be considered,<sup>33,34</sup> hence providing an approximate description in a specific regime of the behavior of cold atoms in one-dimensional optical lattices. This model has also met success in reproducing the different properties regarding the tunneling of Cooper pairs between different superconducting islands in arrays of Josephson junctions.<sup>35</sup> From a technical point of view, note that the model is invariant under global rotations of all the angles—that is, under the global  $U(1)$  symmetry group. A suitable tuning of the parameters defining the model describes then in the thermodynamic limit the evolution towards a quantum phase transition, whose  $U(1)$ -invariant critical point can be described in terms of the conformal field theory of a free scalar field with central charge  $c=1$ , as Ref. 36.

Let us perform now a suitable truncation on the local dimension of the different Hilbert spaces as follows. We choose the individual particle basis of plane waves

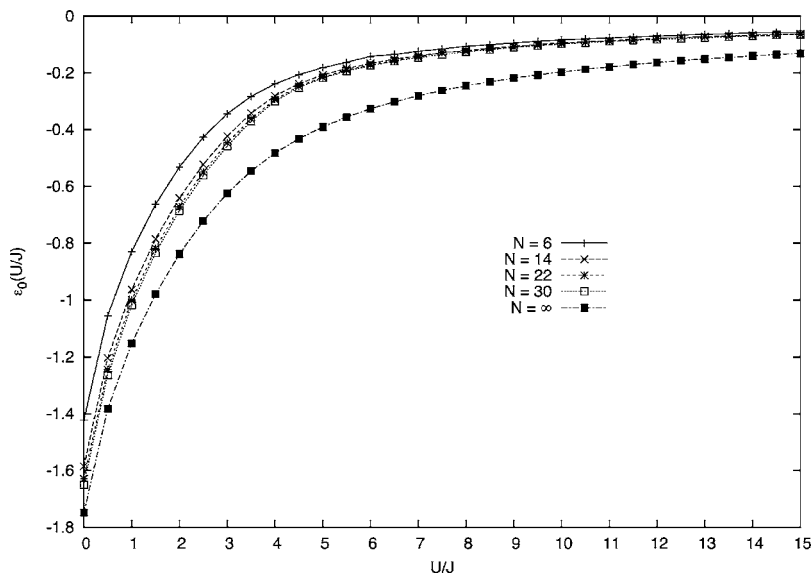


FIG. 9. Energy per lattice site of the ground state for the one-dimensional quantum rotor model, for  $d=7$  and  $\chi=20$ , as computed with MPS algorithms for finite  $N$  and in the thermodynamic limit. Convergence with  $N$  is seen to appear towards the limit  $N \rightarrow \infty$ .

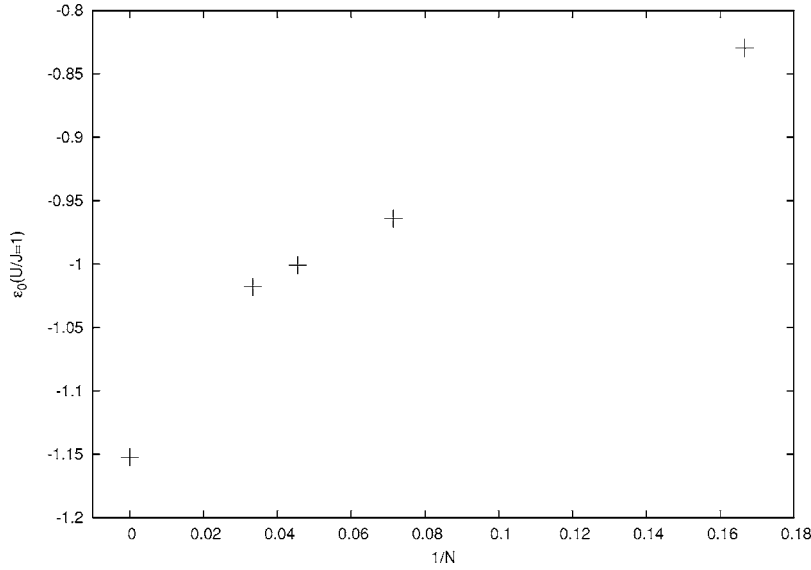


FIG. 10. Convergence with  $N$  of the energy per lattice site of the ground state for the one-dimensional quantum rotor model, for  $d=7$ ,  $\chi=20$ , and  $U/J=1$ , as computed with MPS algorithms for finite  $N$  and in the thermodynamic limit.

$$\phi_{s_k}^{(k)}(\theta_k) = \frac{1}{\sqrt{2\pi}} e^{is_k\theta_k}, \quad (39)$$

with  $s_k = -(d-1)/2, \dots, 0, \dots, (d-1)/2$ , for all the possible  $k$ . Restricted to this truncated basis, the Hamiltonian from Eq. (38) can be expressed as

$$H = \sum_{k=1}^N \left( -2J(V^{(k)}V^{(k+1)} + W^{(k)}W^{(k+1)}) + \frac{U}{2}T^{(k)} \right). \quad (40)$$

The matrix elements of operators  $V$ ,  $W$ , and  $T$  adopt the simple form

$$V_{m,n} = \frac{1}{2}(\delta_{m-1,n} + \delta_{m+1,n}), \quad W_{m,n} = \frac{1}{2i}(\delta_{m-1,n} - \delta_{m+1,n}),$$

$$T_{m,n} = n^2 \delta_{m,n}. \quad (41)$$

Note that for  $d=2$  we have that  $V = \frac{1}{2}\sigma_x$ ,  $W = \frac{1}{2}\sigma_y$ , and  $T = (\sigma_z)^2$ . The truncated Hamiltonian given in Eq. (40) for  $d$

$=2$  then represents a very specific case of the spin-1/2  $XY$  quantum spin chain, which was already known to be an approximation of the one-dimensional Bose-Hubbard model in the Mott insulator regime.<sup>5</sup>

We have performed a variety of calculations over the above-truncated Hamiltonian for several values of the local dimension  $d$  of the Hilbert space by means of the MPS-like algorithms described at the beginning of this work. Our results extend those computed in Ref. 33 and can be understood in terms of the underlying quantum phase transition that the model undergoes in the thermodynamic limit.

#### A. Ground-state energy and entanglement entropy of half a system

We have performed computations of the ground-state energy per lattice site of the system  $\epsilon_0$ , both in the finite-size regime and in the thermodynamic limit, as a function of the ratio  $U/J$ . Initially, we have performed our analysis for a local dimension  $d=7$  and  $\chi=20$ . The results can be found in

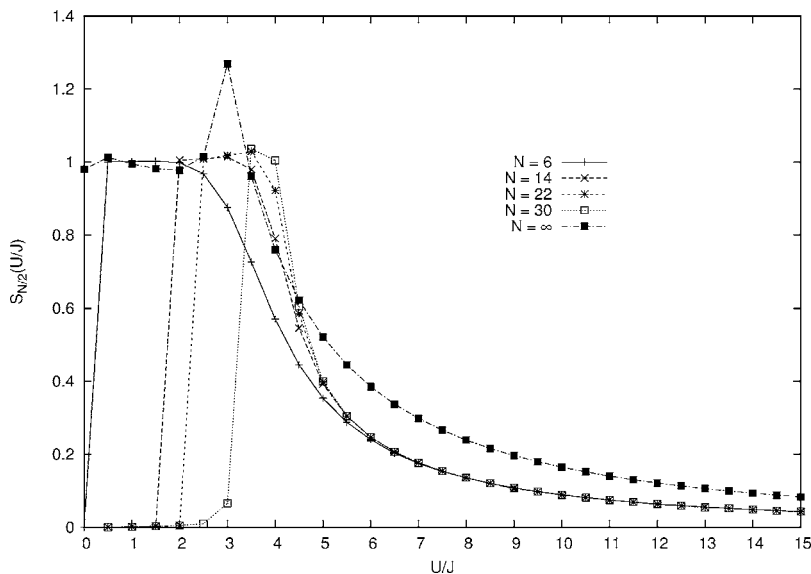


FIG. 11. Entanglement entropy of half a system for the one-dimensional quantum rotor model, for  $d=7$  and  $\chi=20$ , as computed with MPS algorithms for finite  $N$  and in the thermodynamic limit. Spontaneous symmetry breaking of the  $\mathbb{Z}_2$  symmetry of the ground state is observed for the algorithms with finite  $N$  towards the limit  $U/J \rightarrow 0$ , which is not observed in the infinite-size case. This makes the wave function decay from a Greenberger-Horne-Zeilinger- (GHZ-) like superposition of two states to a completely separable state, which results in a null value of the entanglement entropy.

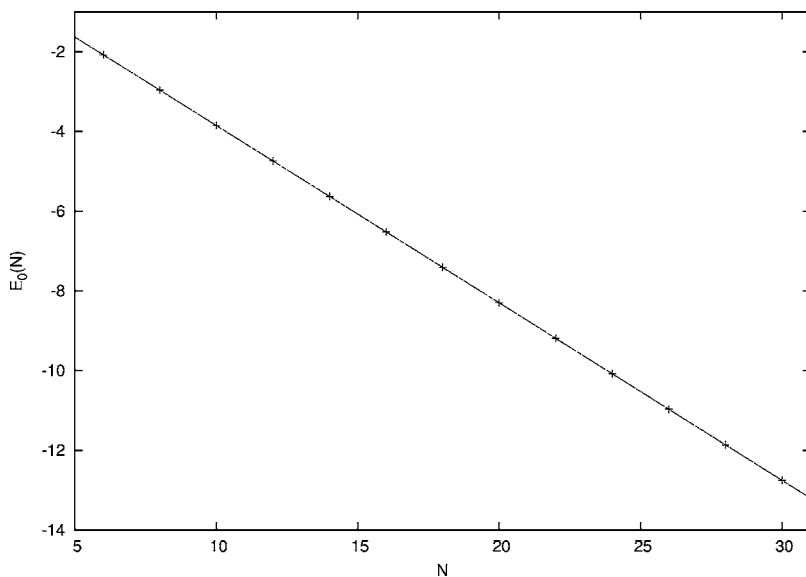


FIG. 12. Finite-size scaling of the ground-state energy at the point of maximum correlations for the one-dimensional quantum rotor model, as computed with MPS algorithms with  $d=14$  and  $\chi=16$ . The line represents the fit to Eq. (42), which provides a value of the central charge of  $c=0.95\pm 0.09$ , which is compatible with the exact value  $c=1$ .

Figs. 9 and 10, which agree with the previous results from Ref. 33 and where it is possible to see the convergence with  $N$  of the ground-state energy found with the algorithms for MPS's with open boundary conditions and for MPS's in the thermodynamic limit.

In order to have a more accurate description of the properties of the ground state close to the critical point, we have performed as well a computation of the entanglement entropy of half a system, as a function of the ratio  $U/J$ , and again both in the finite-size case and the thermodynamic limit. Our results are represented in Fig. 11, which were obtained by using the same values in our MPS techniques as those used in the previous computation of the ground-state energy. According to the maximum observed value of the entanglement entropy, the quantum phase transition appears to be in our infinite-size simulations around  $U/J\sim 3$ , also in accordance with previous estimates from Ref. 33. For finite  $N$ , our MPS numerical algorithms constantly exhibit spontaneous symmetry breaking of the  $\mathbb{Z}_2$  symmetry of the ground state when approaching the limit  $U/J\rightarrow 0$ , which makes the entropy suddenly decrease towards 0 (separable state). The MPS algorithm in the thermodynamic limit has shown to be much more stable in this respect, as it always maintains the GHZ-like superposition in the ground state when approaching the same limit, implying the entropy to evolve towards 1. A divergence in the correlations is also seen to appear when increasing  $N$  at the critical point. However, we can only hint such a divergence because of the finite value of  $\chi$  that we use in our simulations.

### B. Finite-size corrections to the critical ground-state energy

It is possible to make a check of the consistency of the universality class of the model by studying the finite-size corrections of the ground-state energy when close to the critical point. As Ref. 37, for a system with finite size  $N$  and open boundary conditions, the ground-state energy approaches its critical value in the thermodynamic limit in the way dictated by the relation

$$E_0(N) = \epsilon_0(\infty)N + a - \frac{\pi c}{24} \frac{1}{N} + O\left(\frac{1}{N^2}\right), \quad (42)$$

where  $\epsilon_0(\infty)$  is the energy per particle in the continuum limit,  $a$  is a constant, and  $c$  is the central charge describing the underlying universality class of the corresponding conformal field theory in the thermodynamic limit. Fitting the above expression to the ground-state energies computed at the value of maximum entropy for finite  $N$  can then provide us with an estimation of the value for the corresponding central charge  $c$ . Our results for the one-dimensional quantum rotor model can be found in Fig. 12, where we made use of finite- $N$  MPS algorithms with  $d=14$  and  $\chi=16$ . The fit to Eq. (42) is good and provides a value of  $c=0.95\pm 0.09$ , which is to be compared with the exact known value  $c=1$ , corresponding to the  $U(1)$ -invariant critical point.

### C. Spectrum of half an infinite system

We have also performed a numerical evaluation in the thermodynamic limit of the spectrum of the reduced density matrix of half an infinite system. First, the convergence of the spectrum for finite  $\chi=30$  and off-critical  $U/J$  has been considered as the local dimension  $d$  increases. Our results are shown in Fig. 13, where it is possible to observe the convergence in the relative error of each one of the  $\chi$  eigenvalues  $(\lambda_\alpha)^2$  as  $d$  increases. This error is found to be of the order of  $10^{-8}$ . Second, we have performed a computation of the behavior of the spectrum of the half-infinite reduced density matrix as a function of  $U/J$  and away from criticality. In Fig. 14 we show the found results for  $d=7$  and  $\chi=20$ , where a remarkable monotonicity in the eigenvalues and their degeneracies when flowing away from criticality in the parameter space is appreciated. Indeed, it is possible to prove that such a monotonicity is very much related to the preservation of part of the conformal structure of the critical point, when flowing away from criticality in the space of parameters, involving in turn the monotonic majorization of the considered probability distribution.<sup>39–42</sup>

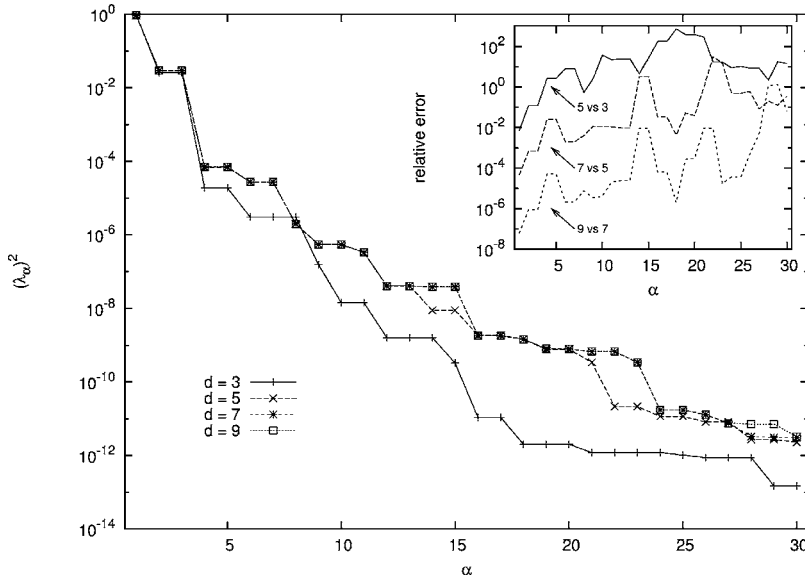


FIG. 13. Spectrum of the reduced density matrix of half an infinite system for the one-dimensional quantum rotor model, as computed with MPS algorithms in the thermodynamic limit and  $\chi=30$ . In the inset, convergence is seen to appear in the relative error of each one of the eigenvalues when increasing the local dimension  $d$ .

## VI. NUMERICAL SOLUTIONS OF PARTIAL DIFFERENTIAL EQUATIONS

The fact that a set of coefficients can be approximated up to some accuracy by means of the contraction of a given tensor network (such as MPS's) has applications well beyond the description of quantum many-body systems, as is the case of the MPS-assisted image compression.<sup>38</sup> In this section we show that the techniques previously introduced can also be used to deal with a purely mathematical problem: namely, that of finding numerical solutions to partial differential equations.

Let  $\Phi(x_1, \dots, x_N)$  denote a function of  $N$  real variables defined on some domain  $\mathcal{D}$ . Let  $\hat{O}$  denote a linear differential operator; that is, we assume that  $\hat{O}$  is some polynomial in  $x_1, \dots, x_N, \partial_{x_1}, \dots, \partial_{x_N}$ . The problem that we consider is to find a numerical solution,  $\Psi(x_1, \dots, x_N)$ , of the equation

$$\hat{O}\Psi + \Phi = 0 \quad (43)$$

on  $\mathcal{D}$ . We suggest that for wide classes of partial differential equations, using  $N$ -variable matrix product functions might turn a powerful computational method. The intuition underlying our point is most simple. A celebrated method to solve partial differential equations is to assume separation of variables—that is, that the solution has the form  $\prod_{i=1}^N \phi^{(i)}(x_i)$ . In the language of quantum information, such a solution would correspond to a pure product state. On the other hand, a fully general solution would have the form

$$\Psi(x_1, \dots, x_N) = \sum_{s_1, \dots, s_N=1}^{\infty} c(s_1, \dots, s_N) \phi_{s_1}^{(1)}(x_1) \cdots \phi_{s_N}^{(N)}(x_N), \quad (44)$$

where the tensor  $c(s_1, \dots, s_N)$  is *a priori* not expected to have

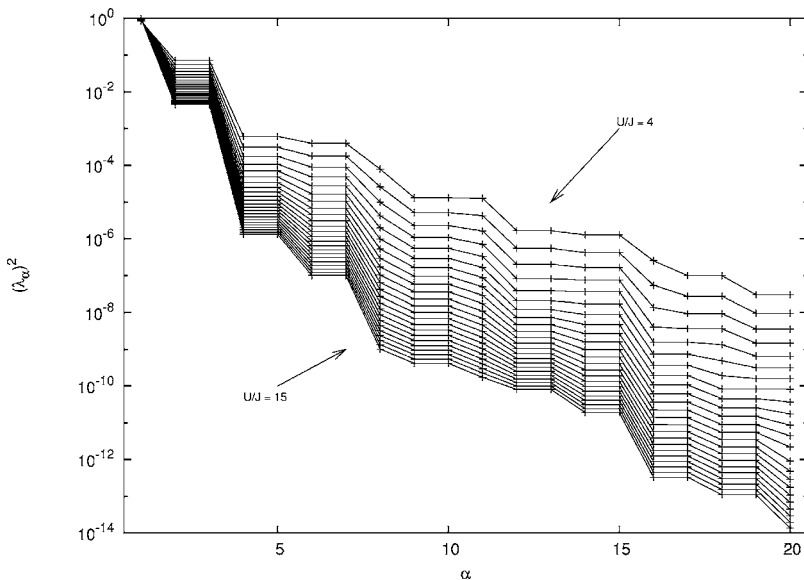


FIG. 14. Spectrum of the reduced density matrix of half an infinite system for the one-dimensional quantum rotor model, as computed with MPS algorithms in the thermodynamic limit with  $d=7$  and  $\chi=20$ , when flowing away from criticality in the ratio  $U/J$ . A remarkable monotonicity in the spectrum is observed.



any particular structure. In the language of quantum information theory, Eq. (44) would correspond to an arbitrary pure entangled state and could be, in principle, exponentially hard to describe as  $N$  grows. Our point is that, in between, the finitely correlated MPS's offer a much more refined description of the solution than the mere separation of variables, *but* still allow for efficient numerical computations.

### A. The algorithm

Let us work in what follows with periodic boundary conditions. In order to find a solution to Eq. (43), we will seek to minimize the error

$$W \equiv \int_{\mathcal{D}} |\hat{\mathcal{O}}\Psi + \Phi|^2. \quad (45)$$

Now observe that if one sees the components of the matrices  $A(k, s_k)$  related to the variable  $k$  as those of a  $d\chi^2$ -component vector  $a_k$ , then  $W$  appears as a positive quadratic form:

$$W = a_k^* \cdot R^{(k)} \cdot a_k + \Gamma^{(k)*} \cdot a_k + a_k^* \cdot \Gamma^{(k)} + \int_{\mathcal{D}} |\Phi|^2, \quad (46)$$

where  $R^{(k)}$  is a  $d\chi^2 \times d\chi^2$  positive matrix and  $\Gamma^{(k)}$  is a  $d\chi^2$  vector. Our algorithm, inspired from those used to find ground states of Hamiltonians described in the previous sections, reads as follows.

- (i) Set the matrices  $A(k, s_k)$  to some initial random values.
- (ii) Sweep through each variable,  $x_k$ , sequentially, and improve the matrices  $A(k, s_k)$  upon solving the linear system of equations

$$R^{(k)} \cdot a_k + \Gamma^{(k)} = 0, \quad (47)$$

until some desired convergence is attained.

At this point, it is worth informing the reader of three useful tricks that help to make the computations well behaved. First, the variables should always be “visited” in the *same* order. For example, if the labels of the variables were arranged on a ring, the matrices related to each variable should always be improved in a clockwise order. Second, we have chosen the random matrices to which the MPS is initialized to be unitary (preconditioning of the solution). Third, after improvement of the matrices related to the  $k$ th variable, we recommend to perform the gauge transformation described in Ref. 7: we compute the singular decomposition  $A(k, s_k)_{\alpha_{k-1}, \alpha_k} = \sum_{\lambda, \mu=1}^{\chi} U_{(s_k \alpha_{k-1}), \lambda}^{(k)} \sum_{\lambda, \mu}^{(k)} W_{\mu, \alpha_k}^{(k)}$  where  $U^{(k)\dagger} U^{(k)} = \mathbb{I}_{\chi}$  and make the gauge transformation  $A(k, s_k)_{\alpha_{k-1}, \alpha_k} \rightarrow U(k, s_k)_{\alpha_{k-1}, \lambda} \equiv U_{(s_k \alpha_{k-1}), \lambda}^{(k)}$ .

### B. An example

We have considered the Poisson equation

$$\Delta\Psi + \Phi = 0, \quad (48)$$

where  $\Delta = \sum_{i=1}^N \frac{\partial^2}{\partial x_i^2}$ . The domain we have considered is  $\mathcal{D} = [0, 1]_1 \times \cdots \times [0, 1]_N$ . As an individual set of functions, we

have chosen plane waves with integer wave index for all possible sites:

$$\phi_{s_k}^{(k)}(x_k) \equiv \phi_{s_k}(x_k) = e^{i2\pi s_k x_k},$$

$$s_k = -(d-1)/2, \dots, (d-1)/2 \quad \forall k. \quad (49)$$

We choose  $\Phi$  to be of the MPS form

$$\begin{aligned} \Phi(x_1, \dots, x_N) &= \sum_{s_1, \dots, s_N = -(d-1)/2}^{(d-1)/2} \text{tr}(F(1, s_1) \cdots F(N, s_N)) \\ &\times \phi_{s_1}(x_1) \cdots \phi_{s_N}(x_N), \end{aligned} \quad (50)$$

where the matrices  $F$  have size  $\chi_{\Phi} \times \chi_{\Phi}$ . Note that taking  $\chi_{\Phi}$  and  $d$  large enough, any (smooth) function  $\Phi$  can be represented in the form (50).

We have performed three different sets of computations for  $N=8, 20$ , and  $40$  variables. All our computations are such that  $\chi_{\Phi}=d$  and such that the matrices  $F$  are chosen to be random and unitary. To fairly evaluate the performance of our algorithm, we define a relative error  $\delta$  as

$$\delta \equiv \frac{\int_{\mathcal{D}} |\hat{\mathcal{O}}\Psi + \Phi|^2}{\sqrt{\int_{\mathcal{D}} |\hat{\mathcal{O}}\Psi|^2 + \int_{\mathcal{D}} |\Phi|^2 + 2\sqrt{\int_{\mathcal{D}} |\hat{\mathcal{O}}\Psi|^2 \times \int_{\mathcal{D}} |\Phi|^2}}}. \quad (51)$$

This definition is inspired by the Cauchy-Schwarz inequality ( $0 \leq \delta \leq 1$ ).

Our results are displayed in Table II. It is remarkable that the relative error decreases approximately exponentially with  $\chi$ .

### C. Including boundary conditions

We have shown how to solve an equation on a given domain without extra constraints. Therefore, the algorithm converges to *some* solution. Still, one often demands to be able to take into account some boundary conditions. Suppose that they are given by a set of  $m$  relations of the form

$$\mathcal{C}_i[\Psi(x_1, \dots, x_N)] + f_i(x_1, \dots, x_N) = 0, \quad (52)$$

where the relation  $i$  is expected to hold on some domain  $\mathcal{D}_i$ ,  $i=1, \dots, m$ . When  $\mathcal{C}_i$  is again of the form poly  $(x_1, \dots, x_N, \partial_{x_1}, \dots, \partial_{x_N})$ , then the boundary condition error

$$W_{\text{BC}} \equiv \sum_i \int_{\mathcal{D}_i} |\mathcal{C}_i[\Psi(x_1, \dots, x_N)] + f_i(x_1, \dots, x_N)|^2 \quad (53)$$

is of the form (46) for some matrices  $R_{\text{BC}}^{(k)}$  and some vectors  $\Gamma_{\text{BC}}^{(k)}$ . So after making the transformation  $R^{(k)} \rightarrow R^{(k)} + R_{\text{BC}}^{(k)}$ ,  $\Gamma^{(k)} \rightarrow \Gamma^{(k)} + \Gamma_{\text{BC}}^{(k)}$ , we see that, with our method, solving a partial differential equation with boundary conditions can be done in exactly the same way as without.

### D. Discussion

Let us now discuss the principal limitations of the methods. First, when the differential operator and the boundary

TABLE II. Performances of the MPS algorithm for solving a Poisson equation.  $N$  denotes the number of variables,  $d$  denotes the number of local levels,  $\chi_\Phi$  is the dimension of matrices  $F$ ,  $\chi$  is the dimension of the matrices of the MPS ansatz,  $W$  is the absolute error, and  $\delta$  is the relative error.

$N$	$d$	$\chi_\Phi$	$\chi$	$W$	$\delta$
8	3	3	3	$3.25 \times 10^{-3}$	$8.13 \times 10^{-4}$
8	3	3	4	$8.4 \times 10^{-4}$	$2.08 \times 10^{-4}$
8	3	3	5	$1.36 \times 10^{-4}$	$3.4 \times 10^{-5}$
8	3	3	6	$4.9 \times 10^{-5}$	$1.23 \times 10^{-5}$
8	3	3	7	$3.4 \times 10^{-5}$	$8.51 \times 10^{-6}$
8	7	7	8	$4.15 \times 10^{-3}$	$1.04 \times 10^{-3}$
8	7	7	9	$3.44 \times 10^{-3}$	$8.61 \times 10^{-4}$
20	5	5	7	$4.4 \times 10^{-4}$	$1.1 \times 10^{-4}$
20	7	7	3	$4.09 \times 10^{-4}$	$1.02 \times 10^{-4}$
20	7	7	4	$3.02 \times 10^{-4}$	$7.56 \times 10^{-5}$
20	7	7	5	$1.2 \times 10^{-4}$	$3 \times 10^{-5}$
20	7	7	6	$9.73 \times 10^{-7}$	$2.43 \times 10^{-7}$
40	3	3	3	$7.3 \times 10^{-5}$	$1.84 \times 10^{-5}$
40	3	3	4	$6.17 \times 10^{-5}$	$1.54 \times 10^{-5}$
40	3	3	5	$3.96 \times 10^{-5}$	$9.9 \times 10^{-6}$
40	5	5	5	$1.58 \times 10^{-4}$	$3.94 \times 10^{-5}$

conditions are not linear, the absolute error is no more of the convenient form (46). More sophisticated methods are then necessary to perform the extremisation.

The second limitation is related to the shape of the domain on which the variables are defined. As a premise to the algorithm, one should calculate tensors of the form

$$G_{i_1, \dots, i_N}^{j_1, \dots, j_N}(\mathcal{O}_1, \dots, \mathcal{O}_N) = \int_{\mathcal{D}} \phi_{j_1}^*(x_1) [\mathcal{O}_1 \phi_{i_1}](x_1) \cdots \phi_{j_N}^*(x_N) \times [\mathcal{O}_N \phi_{i_N}](x_N), \quad (54)$$

where  $\mathcal{O}_1, \dots, \mathcal{O}_N$  are operators related to the variables  $1, \dots, N$ , respectively.

In the example we have treated, the domain was a mere Cartesian product of subdomains, which had allowed us to break  $G$  into pieces  $G_{i_1, \dots, i_N}^{j_1, \dots, j_N}(\mathcal{O}_1, \dots, \mathcal{O}_N) = g_{i_1}^{j_1}(\mathcal{O}_1) \dots g_{i_N}^{j_N}(\mathcal{O}_N)$ . But for an arbitrarily shaped domain, the computational resources (time and memory) necessary to compute  $G$  could grow exponentially with  $N$ . Still the method is not limited to the simplest case where the whole domain could be factored as a product of independent ones. For example, in the case of problems involving relatively small number of variables, this limitation is not so constraining. Second, when  $\mathcal{D}$  can be decomposed as

$$\mathcal{D} = \bigcup_i \mathcal{D}_{i,1} \times \cdots \times \mathcal{D}_{i,n_i}, \quad (55)$$

where each  $\mathcal{D}_{i,j}$  involves a small number of variables, then  $G$  can be decomposed accordingly and thus computed efficiently. These first two comments hold for the boundary conditions as well.

The other drawbacks of the methods are those generally related to MPS algorithms. First, we have no guarantee that the solution provided is a global minimum. However, contrarily to the study of Hamiltonian ground states, we have here a figure of merit that tells us how close to the actual solution the algorithm gets. The second drawback is related to the very structure of the ansatz. When studying many-body quantum systems, it is known that the performance of MPS algorithms in their usual context depends on how far one is from criticality, performing well when the correlations between the particles are finite. In turn we expect our algorithms to behave similarly and to perform poorly for equations which solution are highly entangled functions.

Despite its limitations, it is obvious that the method is very versatile and we believe that it can be successfully applied to a very wide class of differential problems. It certainly deserves further tests on relevant equations as well as theoretical investigation.

## VII. CONCLUSIONS AND OUTLOOK

In this paper we have presented in a pedagogical way several numerical optimization techniques based on MPS's, both for finite systems (with open and periodic boundary conditions) and in the thermodynamic limit. We have shown how these algorithms can be extended in order to study quantum many-body systems with continuous degrees of freedom (continuous variables) by means of appropriate truncations in the local Hilbert spaces. On the one hand, and as a test, we have applied our algorithms to study a finite one-dimensional chain of harmonic oscillators. On the other hand, we have performed a detailed numerical study of the properties of the one-dimensional quantum rotor model. In both cases, we have found high-precision results when working off criticality.

The methods presented in our work can be further applied to the study of different continuous-variable quantum many-body systems. For example, it could be possible to consider the behavior of anyonic excitations in small Bose-Einstein condensates<sup>43</sup> by means of a numerical treatment of Laughlin and Pfaffian wave functions.<sup>44–47</sup> Also, it could be possible to perform a study of systems which alternate both discrete and continuous degrees of freedom, such as spin-boson models.<sup>48</sup> Interacting quantum field theories such as the (1+1)-dimensional  $\lambda\varphi^4$  theory can also be studied by means of these techniques<sup>23</sup> and will be the main topic of a further work.<sup>49</sup>

Clearly, our work can also be extended to alternative tensor networks, such as the two-dimensional projected entangled pair states (PEPS's)<sup>8</sup> or the multi-scale entanglement renormalization ansatz (MERA's).<sup>12</sup> The most delicate point when applying MPS algorithms is probably the choice of a basis. In the case we have treated, the choices (Fock states or plane waves) came quite naturally. But more often than not, to guess a correct single-particle basis in which truncate the Hamiltonian is not an easy business.

Finally, we have exhibited an MPS-like method to solve partial differential equations. The results we have got with the example treated are quite promising, and we hope that

the method will find many applications. Further studies of it are currently under investigation.

#### ACKNOWLEDGMENTS

We thank J. J. García-Ripoll for helpful discussions and

for originally drawing our attention to the quantum rotor model. We also acknowledge MEC (Spain), QAP (EU), Grup Consolidat (Generalitat de Catalunya), and The University of Queensland (Australia) for financial support.

- 
- <sup>1</sup>S. R. White, Phys. Rev. Lett. **69**, 2863 (1992).  
<sup>2</sup>S. R. White, Phys. Rev. B **48**, 10345 (1992).  
<sup>3</sup>U. Schollwoeck, Rev. Mod. Phys. **77**, 259 (2005).  
<sup>4</sup>G. Vidal, Phys. Rev. Lett. **91**, 147902 (2003).  
<sup>5</sup>J. I. Latorre, E. Rico, and G. Vidal, Quantum Inf. Comput. **4**, 048 (2004).  
<sup>6</sup>F. Verstraete and J. I. Cirac, Phys. Rev. B **73**, 094423 (2006).  
<sup>7</sup>F. Verstraete, D. Porras, and J. I. Cirac, Phys. Rev. Lett. **93**, 227205 (2004).  
<sup>8</sup>F. Verstraete and J. I. Cirac, cond-mat/0407066 (unpublished).  
<sup>9</sup>G. Vidal, Phys. Rev. Lett. **93**, 040502 (2004).  
<sup>10</sup>M. Zwoiak and G. Vidal, Phys. Rev. Lett. **93**, 207205 (2004).  
<sup>11</sup>A. J. Daley, C. Kollath, U. Schollwoeck, and G. Vidal, J. Stat. Mech.: Theory Exp. 2004, P04005 (2004).  
<sup>12</sup>G. Vidal, cond-mat/0512165 (unpublished); quant-ph/0610099 (unpublished).  
<sup>13</sup>G. Vidal, Phys. Rev. Lett. **98**, 070201 (2007).  
<sup>14</sup>F. Verstraete, J. J. García-Ripoll, and J. I. Cirac, Phys. Rev. Lett. **93**, 207204 (2004).  
<sup>15</sup>M. C. Bañuls, R. Orús, J. I. Latorre, A. Perez, and P. Ruiz-Femenia, Phys. Rev. A **73**, 022344 (2006).  
<sup>16</sup>V. Murg, F. Verstraete, and J. I. Cirac, Phys. Rev. Lett. **95**, 057206 (2005).  
<sup>17</sup>I. Affleck, T. Kennedy, E. H. Lieb, and H. Tasaki, Phys. Rev. Lett. **59**, 799 (1987).  
<sup>18</sup>I. Affleck, T. Kennedy, E. H. Lieb, and H. Tasaki, Commun. Math. Phys. **115**, 477 (1988).  
<sup>19</sup>S. Ostlund and S. Rommer, Phys. Rev. Lett. **75**, 3537 (1995).  
<sup>20</sup>M. Fannes, B. Nachtergaele, and R. F. Werner, Commun. Math. Phys. **144**, 443 (1992).  
<sup>21</sup>D. Perez-García, F. Verstraete, M. M. Wolf, and J. I. Cirac, quant-ph/0608197 (unpublished).  
<sup>22</sup>W. Lay and J. Rudnick, Phys. Rev. Lett. **88**, 057203 (2002).  
<sup>23</sup>T. Sugihara, J. High Energy Phys. **05**, 007 (2004).  
<sup>24</sup>T. Sugihara, J. High Energy Phys. **07**, 022 (2005).  
<sup>25</sup>N. Schuch, J. I. Cirac, and M. M. Wolf, Commun. Math. Phys. **267**, 65 (2006).  
<sup>26</sup>M. Suzuki, Phys. Lett. A **146**, 319 (1990); J. Math. Phys. **32**, 400 (1991).  
<sup>27</sup>M. Cramer, J. Eisert, M. B. Plenio, and J. Dreissig, Phys. Rev. A **73**, 012309 (2006); K. Audenaert, J. Eisert, M. B. Plenio, and R. F. Werner, *ibid.* **66**, 042327 (2002); Alonso Botero and Benni Reznik, *ibid.* **70**, 052329 (2004).  
<sup>28</sup>C. Zhang, E. Jeckelmann, and S. R. White, Phys. Rev. Lett. **80**, 2661 (1998).  
<sup>29</sup>L. G. Caron and S. Moukouri, Phys. Rev. B **56**, R8471 (1997).  
<sup>30</sup>I. Peschel and M. Chung, J. Phys. A **32**, 8419 (1999).  
<sup>31</sup>M. Luscher, Nucl. Phys. B **254**, 52 (1985); M. Srednicki, Phys. Rev. Lett. **71**, 666 (1993).  
<sup>32</sup>*Handbook of Mathematical Functions*, edited by M. Abramowitz and I. A. Stegun (Dover, New York, 1965).  
<sup>33</sup>J. J. García-Ripoll, J. I. Cirac, P. Zoller, C. Kollath, U. Schollwoeck, and J. von Delft, Opt. Express **12**, 42 (2004).  
<sup>34</sup>M. P. A. Fisher, P. B. Weichman, G. Grinstein, and D. S. Fisher, Phys. Rev. B **40**, 546 (1989).  
<sup>35</sup>R. Fazio and H. van de Zant, Phys. Rep. **355**, 235 (2001) and references therein.  
<sup>36</sup>I. Affleck, Phys. Rev. Lett. **55**, 13 (1985).  
<sup>37</sup>H. W. Blöte, J. L. Cardy, and M. P. Nightingale, Phys. Rev. Lett. **56**, 7 (1986).  
<sup>38</sup>J. I. Latorre, quant-ph/0510031 (unpublished).  
<sup>39</sup>J. I. Latorre, C. A. Lutken, E. Rico, and G. Vidal, Phys. Rev. A **71**, 034301 (2005).  
<sup>40</sup>R. Orús, Phys. Rev. A **71**, 052327 (2005); **73**, 019904(E) (2006).  
<sup>41</sup>H. Zhou, T. Barthel, J. O. Fjaerstad, and U. Schollwoeck, Phys. Rev. A **74**, 050305(R) (2006).  
<sup>42</sup>R. Orús (unpublished).  
<sup>43</sup>B. Paredes, P. Fedichev, J. I. Cirac, and P. Zoller, cond-mat/0103251 (unpublished).  
<sup>44</sup>R. B. Laughlin, Phys. Rev. Lett. **50**, 1395 (1983).  
<sup>45</sup>S. Iblisdir, J. I. Latorre, and R. Orús, Phys. Rev. Lett. **98**, 060402 (2007).  
<sup>46</sup>M. Haque, O. Zozulya, and K. Schoutens, Phys. Rev. Lett. **98**, 060401 (2007).  
<sup>47</sup>B. Paredes, T. Keilmann, and J. I. Cirac, cond-mat/0608012 (unpublished).  
<sup>48</sup>N. Lambert, C. Emary, and T. Brandes, Phys. Rev. Lett. **92**, 073602 (2004).  
<sup>49</sup>R. Orús, S. Iblisdir, and J. I. Latorre (unpublished).